ChemPhysChem

Research Article
doi.org/10.1002/cphc.202400329

Chemistry Europe
European Chemical Societies Publishing

www.chemphyschem.org

Deciphering Pyramidanes: A Quantum Chemical Topology Approach

Lucía Vidal[+],[a, b] Daniel Barrena-Espés[+],[a] Jorge Echeverría,[b] Julen Munárriz,*[c] and Ángel Martín Pendás*[a]

$C[C_4H_4]$, the simplest compound of the [4]-pyramidane family, has so far eluded experimental characterization, although several of its analogs, $E[C_4(SiMe_3)_4]$ in which the E apex atom is a tetrel group element, have been successfully prepared. The non-classical bonding mode of E, similar to that found in propellanes, has prompted a considerable number of theoretical studies to unravel the nature of the apex-base interaction. Here, we contribute to this knowledge by analyzing the electron localization function (ELF) and classical QTAIM descriptors; as well the statistical distribution of electrons in atomic regions by means of the so-called electron distribution functions (EDFs), calculation of multicenter indices (MCI) as aromaticity descriptors and by performing orbital invariant energy decompositions with the interacting quantum atoms (IQA) approach on a series of $E[C_4(SiMe_3)_4]$ compounds. We find that the bonding evolves from covalent to electrostatic as E changes from C to Pb, with an anomaly when E=Si, which is shown to be the most charged moiety, compatible with an aromatic $[C_4(SiMe_3)_4]^{2-}$ scaffold in the pyramidane base.

Introduction

The design and synthesis of molecular structures imitating captivating objects with exotic properties has consistently been a wellspring of inspiration for chemists.[1] In this regard, pyramids are mesmerizing objects that have always been a source of fascination for humanity. It is not surprising, therefore, that there has been a prolonged quest for synthesizing molecular compounds with pyramid-like geometries, commonly known as pyramidanes. Compounds of this nature, featuring a trigonal to hexagonal pyramid structure, may either consist of a purely carbon-based skeleton (often existing solely as theoretical constructs) or include an electronically equivalent main group element at one or more vertices.[2]

In this contribution, we report on tetragonal pyramid compounds, commonly known as [4]-pyramidanes (where '4' denotes the number of atoms in the base),[2] or more frequently just as pyramidanes. The nomenclature for this novel class of main group-based clusters stems from the partner compound, the simplest all-carbon system exhibiting a square planar pyramid geometry, $C[C_4H_4]$ (Chart 1) which is generally known as *pyramidane* (with the IUPAC name being tetracyclo-[2.1.0.0^{1,3}.0^{2,5}]pentane).[3] This geometric arrangement involves the apex carbon atom in a tetracoordinate geometry distinct from the tetrahedral one, an example of an inverted tetrahedral (or *"umbrella"*) configuration –a bonding mode also observed in the extensively studied *propellane* family.[4]

The stability of $C[C_4H_4]$ has undergone comprehensive theoretical scrutiny since the late seventies, employing a spectrum of methodologies, including semiempirical, HF, MP2, DFT, and CCSD(T) levels of theory.[5–10] Predictions derived from these studies consistently affirm that it represents a stable minimum on the potential energy surface (PES), exhibiting kinetic stability against ring-opening processes. However, despite these theoretical assertions, its elusive nature persists to date.

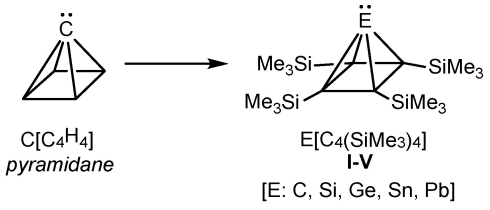

Chart 1. Parent pyramidane compound and derivatives studied in this contribution.

In contrast, various analogues to $C[C_4H_4]$, wherein the vertex is substituted with a formally isoelectronic group 14 element, have been successfully isolated and characterized.[11] Notably, this set encompasses species such as $E[C_4(SiMe_3)_4]$ with E=Si

[a] L. Vidal,[+] D. Barrena-Espés,[+] Á. M. Pendás
Departamento de Química Física y Analítica, Universidad de Oviedo, Julián Clavería 8, Oviedo 33006, Spain
E-mail: ampendas@uniovi.es

[b] L. Vidal,[+] J. Echeverría
Departamento de Química Inorgánica and Instituto de Síntesis Química y Catálisis Homogénea (ISQCH), Universidad de Zaragoza, Pedro Cerbuna 12, Zaragoza 50009, Spain

[c] J. Munárriz
Departamento de Química Física and Instituto de Biocomputación y Física de Sistemas Complejos (BIFI), Universidad de Zaragoza, Pedro Cerbuna 12, Zaragoza 50009, Spain
E-mail: julen@unizar.es

[+] These authors contributed equally.

Supporting information for this article is available on the WWW under https://doi.org/10.1002/cphc.202400329

(**II**),[12] Ge (**III**), Sn (**IV**),[13] and Pb (**V**),[14] as illustrated in Chart 1, while the carbon-based analogue (**I**) remains inaccessible. Such family constitutes the central theme of this contribution as it will be explained later. Exotic pentagerma- and pentastannapyramidane species have also been prepared by Lee *et al*,[14] as well as other derivatives in which carbon atoms of the pyramid base are substituted by phosphorous.[15,16]

Another relevant isoelectronic analogue is that in which the C apex is replaced by a C–H group, the final moiety being thus positively charged. While $(CH)[C_4H_4]^+$ has not been isolated, a methyl disubstituted derivative has been obtained when working in superacidic medium (SO_2ClF/FSO_3H, 3 : 2).[17,18] In this direction, isoelectronic cationic phosphapyramidanes have also been prepared, including examples with a phosphorous atom at the apex.[19] Consistent with these findings, replacement of the $(CH)^+$ apex with a B–R functional group (also isoelectronic to E) has resulted in several instances of the so-called borapyramidanes. Intriguingly, these structures have demonstrated interconversion with their planar 5–member borole analogues through thermolysis[20] or reduction processes.[21] Notably, the latter leads to the formation of the corresponding 6-π aromatic ring, featuring two negative charges. Such kind of transformation has also been reported for a phosphorous-substituted germapyramidane,[15] and has been the subject of theoretical examination.[22]

Be that as it may, considering the aforementioned non-classical bonding mode exhibited by the apex atom, there has been a concentrated effort to understand both the nature of the apex–base interaction and the chemical bonding within the base.[11] Theoretical investigations encompass the analysis of canonical molecular orbitals (MOs), natural bond orbitals (NBOs), and Wiberg bond indices; in addition to the examination of electron density and related scalar fields, including its Laplacian, within the Quantum Theory of Atoms in Molecules (QTAIM)[23] formalism.[13,14,19,24,25] Moreover, other scalar fields defined in real space, such as the Electron Localization Function (ELF),[26] have been employed.[13,20] The four-membered base ring has also been proposed to exhibit a significant aromatic character[2,14,19] on the basis of its MOs and negative nucleus-independent chemical shifts (NICS) and $NICS(1)_{zz}$.[27] More recently, the energy decomposition analysis with natural orbitals for chemical valence[28] (EDA-NOCV) has been applied to the silapyramidane **II**.[12] These studies indicate covalent bonding between the adjacent carbon atoms comprising the base, while the interaction between the apex and the base is primarily governed by electrostatic interactions. The only exception is the case of the carbon analogue (**I**), for which this interaction would still be covalent; although the bonding descriptors (such as Wiberg bond indices and C–C distances) indicate a bond order lower than 1, revealing that it is not a classic two-center two-electron bond.[13] Such finding agrees with experimental observations, based on NMR and Mössbauer spectroscopy, in addition to X-ray crystallograpgy.[14] As a result, group 14 pyramidanes (**III–V**, E=Ge, Sn, Pb) have been proposed to be better described as a properly weighted resonance between covalent and ionic forms, as shown in Scheme 1.[13,14] Solely based on naïve analyses of these resonance forms,

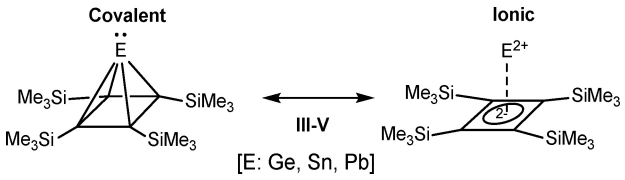

Scheme 1. Proposed resonance forms for pyramidanes **III** to **V**.

several structural and electronic properties, among which we simply mention the deviation from planarity of the C_4–Si_4 scaffold or its degree of aromaticity, can be attributed to a change in the weight of the covalent/ionic contributions. In this regard, we should mention that the bonding in these systems can be rationalized by resorting to the Wade-Mingos-Rudolph rules, as pyramidanes can be considered as *nido*-cluster compounds with *n* framework atoms.[29] Their electronic framework is formed by $(n+2)$ binding electron pairs, and they have a total of 5 framework atoms, which leads to 7 electron pairs. As 4 pairs are assigned to the σ-bond framework of the base, the apex–base interaction (including five centers) is formed by 6 electrons (3 pairs), pointing to a delocalized bonding character and to a formal bond order equal to $^3/_4$ for each of these interactions.[2]

It is also worth noting that pyramidanes can, at least formally, be considered as derivatives of a cyclobutadienyl-based scaffold coordinated to a p-block atom located at the apex. This observation holds significance, as complexes involving s-,[30] d-,[31] and f-block[32] elements are abundant, while examples involving p-block atoms are still very scarce. This way, the predominance of the ionic resonance forms in several pyramidanes could set the stage for the synthesis of analogs resembling cyclobutadienyl structures, $[(CR_3)_4]^{2-}$.[13,14]

It is our purpose to further contribute to their understanding by applying state-of-the-art real-space techniques included within the Quantum Chemical Topology (QCT) framework.[33] For that, we resorted to the Interacting Quantum Atoms (IQA) energy decomposition scheme.[34] In our view, this methodology offers an important advantage over other energy decomposition schemes as it relies on orbital invariant quantities (the reduced first-order density matrix and the pair density), remaining independent of any arbitrary reference state. Furthermore, it rigorously partitions the system's energy into physically meaningful components and enables the decomposition of interactions between two atoms or groups of atoms. This decomposition results in a classical term (V_{cl}), typically associated with the electrostatic contribution of the interaction, and an exchange-correlation term (V_{xc}), which is considered as its covalent counterpart.[35] Amidst various applications that have been recently reviewed,[36] the relevance of IQA is particularly pronounced in characterizing exotic interactions. This encompasses interactions like those between Co/Mn and pentafluoroorthotellurate groups,[37] aurophilic and argentophilic interactions,[38] and the recently proposed, albeit not exempt from controversy, collective interactions among organometallic compounds.[39] We also evaluated two- and multicenter bond orders. The two-center delocalization index (DI)

between QTAIM basins (either atomic or those corresponding to functional groups) can be interpreted as the number of electron pairs shared by two basins and is considered as the real space analog of the bond order.[40] The DI is directly related to V_{xc}, in such a way that, to a zero-th order approximation, $V_{xc} \approx -\frac{DI}{2R}$.[41] Similarly, the multicenter index, MCI, provides a quantification of the multicenter bond order that exists between a set of atoms or groups, and can be applied as a measure of aromaticity.[42]

We integrated the previous approaches with the statistical interpretation of chemical bonding provided by the so-called electron distribution functions (EDFs),[43] which provide the probability of finding a given partition of the N electrons of a molecule in a set of predefined spatial regions that fill the space. By using a QTAIM decomposition, we can determine the probability of locating a specific distribution of the electrons into the atoms or functional groups we are interested in. This methodology recovers an appealing, comprehensive, and chemically insightful depiction of the system's chemical bonds.[44]

We have selected systems **I–V** (Chart 1) as illustrative instances of the pyramidane family: **II–V** are among the few synthesized pyramidane examples, while **I** is identified as a coveted long-term synthetic target. Furthermore, the apex of the pyramid, the E atom, encompasses the five most significant representatives of Group 14. For the sake of comparison, we have also analyzed the analogous systems in which the trimethylsilyl (TMS) group has been substituted by H and SiH_3 groups. This way, the study of these systems enables us to meticulously analyze the evolution of the E–base bonding pattern as we traverse Group 14 and examine its influence on its bonding within the base.

Results and Discussion

We first conducted structure optimizations for compounds **I–V** utilizing the B3LYP–D3BJ/def2-TZVP level of theory. In this regard, we note that we also tested other DFT functionals (M06, M06–L and TPSSh), and all of them provided consistent results, as explained in the Computational Details section and the Supporting Information. This way, we selected B3LYP method, which has also been applied by some of us in IQA and EDF studies, yielding insightful and consistent results.[37,45] To our surprise, our investigation unveiled the presence of two distinct local minima, each characterized by the arrangement of the trimethylsilyl substituents at the base of the pyramid, as illustrated in Figure 1. This conformational flexibility seems to have been overlooked in previous theoretical studies. In the first geometrical scenario, denoted as #1, the C–C–Si angles pair off evenly, with TMS groups positioned in opposite planes at adjacent corners, resulting in a system's symmetry akin to C_{2v}. Conversely, in the alternative configuration #2, all C–C–Si angles are identical, and the TMS groups are situated behind the base plane relative to the E atom, showcasing an approximate C_{4v} symmetry. The electronic energy differences between structures #1 and #2 are very small, as shown in Table 1, structure #1 being more stable in **I** (3.7 kcal mol^{-1}), **II** (0.5 kcal mol^{-1}) and **III** (0.2 kcal mol^{-1}), while possibility #2 would be preferred in **IV** and **V** (in both cases by about a marginal energy difference of 0.5 kcal mol^{-1}).

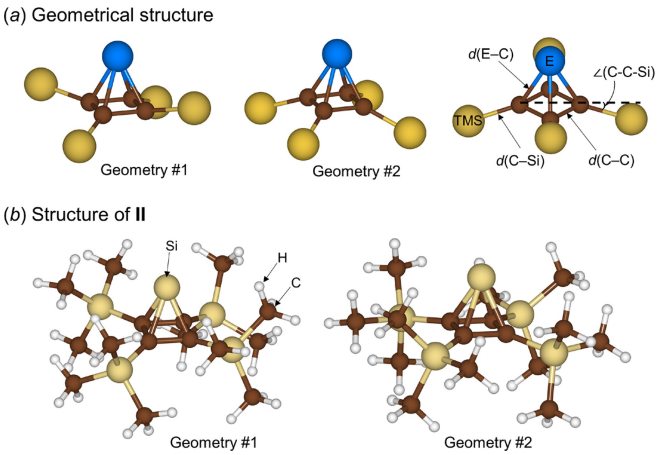

Figure 1. (*a*) Possible geometrical structures obtained for compounds **I–V** and $[C_4(SiMe_3)_4]^{2-}$ and geometrical parameters depicted in Table 1. (*b*) B3LYP–D3BJ optimized geometrical structures for system **II**.

To validate our findings, we conducted supplementary calculations employing the M06, M06–L, and TPSSh exchange–correlation functionals, which consistently corroborated our observations, (see Tables S1–S4 provided in the Supporting Information). Moreover, an analysis of the crystallographic structures of **II–V**, revealed that, in the four cases, the geometrical structures correspond to #1.[12–14] This finding agrees with our calculations, especially after considering that crystal packing effects can favor structural arrangement #1 in cases where it is slightly less favored in the gas-phase (as in **IV** and **V**). Given the very small energy difference between both structures, we expect a dynamic equilibrium between them in solution.

We consider that the steric hindrance due to the disposition of bulky TMS groups plays an important role in the appearance of both potential geometries. However, electronic effects should not be overlooked. In this regard, we note that the structure of closely related cyclobutadiene-based anions

Table 1. Main geometrical parameters for systems **I–V** and $[C_4(SiMe_3)_4]^{2-}$ when their geometrical structure corresponds to alternative #1.

System	d(E–C)/Å	d(C–C)/Å	∠(Si–C–C)′
I	1.653	1.466	5.3
	1.650		−14.6
II	2.036	1.478	13.1
	2.033	1.477	−4.0
III	2.155	1.479	13.8
	2.147	1.477	−2.8
IV	2.362	1.478	15.5
	2.356	1.480	−0.4
V	2.463	1.479	15.4
	2.456	1.477	−1.4
$[C_4(SiMe_3)_4]^{2-}$	–	1.475	11.0
		1.477	−11.0

$[(CR_3)_4]^{2-}$ has been subjected to significant investigations by means of theoretical calculations. They have shown that the most stable structure does not correspond to a configuration where all substituents align within the molecular plane, which would correspond to a completely delocalized structure with D_{4h} symmetry. Instead, it is found in configurations exhibiting closer-to-C_{2h} symmetry (depending on the substituent), where two substituents positioned non-consecutively extend above the plane, while the remaining two are situated behind it.[46] This effect has been attributed to impact of the repulsive interactions within the ring members, which reduces the aromatic character of the ring.[46e] In the light of the geometrical structure of pyramidanes **I–V**, such effect is also expected to be present to some extent in these systems. In this line, and for the sake of comparison, we computed the structure of $[C_4(SiMe_3)_4]^{2-}$ anion, which presents a similar scenario that includes two potential structures. One exhibits a distorted configuration where TMS groups are positioned above and behind the molecular plane in even pairs (associated with #1), while the other features a completely planar molecular skeleton. The former is 1.3 kcal mol^{-1} more stable.

We compared the previous systems with the ones that occurs when bulky TMS groups are replaced by the much less encumbered hydrogen ($E[C_4H_4]$, denoted as $\mathbf{I_a}$–$\mathbf{V_a}$) and silyl ($E[C_4(SiH_3)_4]$, denoted as $\mathbf{I_b}$–$\mathbf{V_b}$) substituents. In both cases, only one type of geometry was obtained, which is like geometry #2 in pyramidanes **I–V**; that is, all the E–C–H or E–C–Si angles are similar. Moreover, the E–C distance in the three sets of systems were very similar to each other, as shown in Table S7. In broad strokes, this finding supports the relevant effect of steric repulsion in the appearance of two potential molecular geometries in **I–V**.

Turning back to **I–V**, their geometrical parameters, as well as those of $[C_4(SiMe_3)_4]^{2-}$, are summarized in Table 1, and will be succinctly discussed. We only focus on results for experimentally observed geometry #1 analogues, while the results for #2 are provided in the Supporting Information (Table S6). In this respect, note that while for geometry #2 all E–C and C–C distances are equal, for geometry #1, they are equal by pairs, because of the breaking of the C_{4v} symmetry (to an approximate C_{2v} one) due to TMS orientation.

Initially noticeable is the trend in the C–C–Si angle, which opens to more positive values –we have set the positive directionality when the E atom and the TMS groups are positioned on opposite sides of the base plane. This shift reflects the mounting steric hindrance between E and TMS as the atomic number of E rises and its electron cloud expands, and, in broad strokes, accounts for the relative stabilization of geometry #2.

The E–C and C–C distances exhibit remarkable similarity across both potential geometries. Therefore, only those pertaining to the experimentally observed #1 alternative warrant discussion. As expected, the E–C distance increases when increasing the atomic number of E; and it is also longer than typical purely covalent E–C bonds. For instance, for **I** (E=C) the distance lies in the range 1.650–1.653 Å; while in standard single C–C bonds it typically hovers around 1.54 Å.[47] This reflects the considerable strain present in this non-classical bond. For silapyramidane **II**, the computed E–C distance lies between 2.033 and 2.036 Å, being considerably larger than in classical Si–C bonds,[47] and pointing also towards significant electrostatic character. The same idea applies to **III–V**, for which the E–C distances are about 2.15 Å (**III**), 2.36 Å (**IV**) and 2.46 Å (**V**), while covalent distances computed on the basis of covalent radii would be around 1.95 Å (**III**), 2.15 Å (**IV**) and 2.19 Å (**V**), respectively. Note that our calculated bond distances agree well with reported values for **II**,[12] **III**,[14] **IV**[13] and **V**.[14]

Another aspect to consider is the evolution of the C–C distance within the base. To evaluate the influence of the apex atom on the base's electronic structure, we compare these distances with those observed in $[C_4(SiMe_3)_4]^{2-}$ system. This molecule represents the extreme scenario of very polar bonding (in which the E atom would donate two electrons to the base), as depicted in the ionic resonance form in Scheme 1. It has a C–C distance of 1.475–1.477 Å (due to the distortions created by the steric repulsions of TMS groups). Notice that the C–C distance in **I** (1.466 Å) deviates slightly from the values above, while those in **II–V** closely approach the previous value, as well as those of Li and Mg aromatic complexes with the cycobutadiene dianion,[30] providing evidence for a significant electrostatic component in this interaction and also for the aromatic character of the base, as previously put forward by Minayev *et al.*[13]

To provide further information on the bonding pattern exhibited by these systems, we computed QTAIM charges (see Table 2). As is well known, atomic charges are not directly related to oxidation states, but provide a relevant average of the atom-in-the-molecule electronic structure. Although it might be a matter of debate, we have chosen QTAIM charges for consistency. Other possibilities, like the NPA charges of Weinhold and coworkers[48] have also been heavily criticized.[49] In this regard, the E–C bond in **I** is expected to be mainly covalent, and its charge is small, −0.19 a.u. On the contrary, the charges of **II–V** are significantly positive, with two clearly different groups: the charge of **II** is +1.04 a.u., and that of **III–V** is about +0.6 a.u. (+0.63 for **III**, +0.65 for **IV** and +0.59 for **V**). This indicates a higher polar character for **II** than for **III–V**.

The Molecular Electrostatic Potentials (MEP) of the $E[C_4H_4]$ model systems is provided in Figure S4, and they clearly reveal the different charges of the E atom in **I** and **II–V**. Namely, the MEP (mapped onto a $\rho = 0.001$ a.u. surface) at the apex becomes positive after Si, and its most negative site lies at the center of the $[C_4H_4]$ moiety in all systems but $\mathbf{I_a}$ ($C[C_4H_4]$).

A much more detailed image can be provided by dissecting these charges through a QTAIM/EDF analysis. For instance, q(E) is a weighted sum of all the possible electron counts of atom E, the weights being the probability of finding a particular number of electrons in the QTAIM atomic region associated to E.[43,44] We refer to the different possible distributions of the N electrons within the molecule as a Real Space Resonance Structure (RSRS); each of which is linked to a specific probability, p(S).[50] The distribution function of the RSRSs is called the Electron Distribution Function, and provides a chemically intuitive representation of chemical bonding, in such a way that a

Table 2. QTAIM charges for E atom in pyramidanes **I–V**, and selected delocalization indices and IQA interaction terms (values in kcal mol^{-1}) for **I–V** (geometry #1) and $[C_4(SiMe_3)_4]^{2-}$. Note that, given the asymmetry of pyramidanes, the E–C and C–C′ terms were equal by even pairs, although very similar to each other; that is why mean values are reported.

	q(E)	E–[$C_4(SiMe_3)_4$]				E–C		C–C		C–C′	
		E_{int}	V_{cl}	V_{xc}	DI	V_{xc}	DI	V_{xc}	DI	V_{xc}	DI
I	−0.19	−439.8	38.5	−478.3	3.24	−115.1	0.75	−206.2	1.11	−15.7	0.18
II	1.04	−635.0	−397.9	−237.1	2.13	−55.6	0.48	−226.6	1.24	−19.4	0.22
III	0.63	−384.2	−112.8	−271.4	2.50	−63.8	0.57	−218.9	1.20	−15.7	0.19
IV	0.65	−341.1	−97.4	−243.7	2.46	−56.7	0.55	−218.1	1.20	−16.6	0.19
V	0.59	−298.9	−65.0	−233.9	2.48	−54.3	0.55	−217.4	1.19	−16.0	0.18
$[C_4(SiMe_3)_4]^{2-}$	–	–	–	–	–	–	–	−224.4	1.28	−20.3	0.26

system characterized by a broad RSRS distribution is associated with higher covalency due to increased electron delocalization. Conversely, a sharper distribution is indicative of highly polar bonding regimes where electrons tend to localize around specific centers. In this regard, the position of the number of electrons assigned to the probability peak is also indicative of the electronegativity, given that more electronegative regions attract more electrons.[44]

We partitioned the system into two different regions: the E atom and the cyclobutadiene-based base, the results being provided in Figure 2. Note that we comment on the results involving geometry #1, those corresponding to #2 being provided in the Supporting Information (Figure S1). Nonetheless, the differences on the EDF results between both geometric patterns are marginal, and the same outcomes are obtained regardless of the chosen geometry. In order to compare results among systems with different number of electrons in the inner shells, (the E atom belongs to a different period for each system), only *n*s and *n*p valence electrons of E atoms are reported in Figure 2. That is, the neutral E atom would have 4 valence electrons in all cases.

The EDF analysis reveals two differentiated behaviors: for **I**, a nearly symmetric RSRS distribution is found, the probability peak ($p = 0.306$) being located at 4 electrons (i.e. the valence electrons of neutral C atom), which corresponds to the $C^0[C_4(SiMe_3)_4]^0$ RSRS. The following distributions, ordered by relevance, are those in which 5 electrons are hosted in E, $C^+[C_4(SiMe_3)_4]^-$, with a probability of 0.240, and the inverse one, in which 3 electrons are found in the apex atom: $C^-[EC_4(SiMe_3)_4]^+$, with a nearly equal probability of 0.221. Such wide and relatively symmetrical distribution centered at the $C^0[C_4(SiMe_3)_4]^0$ RSRS is indicative of a highly covalent regime,[44] in which electrons are exchanged (shared) among E and the base. Nonetheless, there is some asymmetry in the distribution, clearly skewed to numbers of electrons larger than four (shifter to the right in Figure 2), which results in the final small negative charge of the apex C atom in **I**.

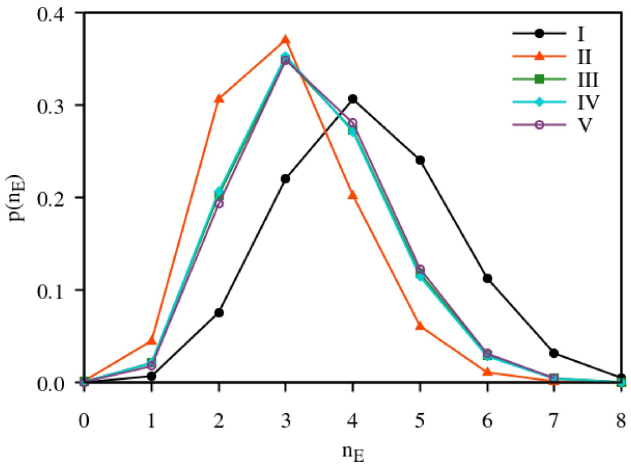

Figure 2. Two-domain EDF for the pyramidanes under study (**I–V**, geometry #1). The probability that a given number of valence electrons be found in the E atom is plotted against the number of electrons.

On the contrary, for **II–V** the probability peak shifts to 3 valence electrons in the E atom, that is, to the $E^+[C_4(SiMe_3)_4]^-$ RSRS; with a probability that is similar in the four cases: 0.371 for silapyramidane **II**, and about 0.35 for compounds **III–V**. This result points towards a considerably more polar bonding regime in the latter. Nonetheless, there are significant differences within the **II–V** systems. Namely, while the EDFs of **III**, **IV** and **V** are nearly indistinguishable from each other (green, blue, and purple lines in Figure 2), that of **II** (depicted in orange) shows a significantly different profile, being shifted to the left (that is, to a lower number of electrons in the E atom).

More specifically, while the distribution with 4 electrons in the E atom, $E^0[C_4(SiMe_3)_4]^0$, is ranked second in **III–V** (E: Ge, Sn, Pb), with probabilities about 0.275; for **II**, the second most probable RSRS is that with only 2 electrons in Si (the $Si^{2+}[C_4(SiMe_3)_4]^{2-}$ RSRS, with a probability of 0.307), the RSRS with 4 electrons in Si ($Si^0[C_4(SiMe_3)_4]^0$) having a much lower probability of 0.202. These results correlate with the ones derived from the charges, showing a significantly different bonding pattern in **II**, in line with the well-known specific chemistry of silicon in the tetrel group.[51]

In passing, it is noticeable to remark that EDF distribution of $E[C_4H_4]$ and $E[C_4(SiH_3)_4]$ systems (provided in Figures S2 and S8, respectively) is virtually identical to that of $E[C_4(SiMe_3)_4]$, which provides further evidence that the effect of the TMS groups on the structure of the considered pyramidanes is steric (rather than electronic).

To attain a rigorous assessment of the energetic signature of the previous results, we resorted to an IQA analysis.[34] As we are interested in electron sharing interactions (associated to the covalent counterpart of the interaction), we base our analysis on the V_{xc} component. It has been proposed to be a reliable indicator of bond strength, as its classical counterpart (V_{cl}) is affected by the long-range character of electrostatic interactions.[35] This way, we report V_{cl} and E_{int} only for the whole E–[$C_4(SiMe_3)_4$] interaction, for which charge separation is more relevant, while for specific interactions we rely on the V_{xc} term only. In order to analyze in detail the effect of the apex atom on the structure of the cyclobutadiene-based pyramidane base, we also include the results for the $[C_4(SiMe_3)_4]^{2-}$ anion, taken as a reference. As for the previous discussion, the results corresponding to conformation #1 are presented and explained in the main text (Table 2), while those corresponding to #2 are provided in the Supporting Information (Table S7). Both datasets lead to the same conclusions.

When examining the E–[$C_4(SiMe_3)_4$] interaction, a notable observation is the destabilizing nature of the V_{cl} term in **I**, contrasting with its stabilizing nature in all other cases. This is again characteristic of a very weakly polar covalent bonding regime between basically neutral moieties in **I**, wherein the interaction is sustained through electron-sharing interactions, represented by V_{xc}. Conversely, the classical interaction is clearly stabilizing in **II–V**, in agreement with the charge separation between the apex (E atom) and the base ($C_4(SiMe_3)_4$ scaffold). The strength of the classical interaction peaks in silapyramidane **II**, owing to its highly positive charge on E. Subsequently, this intensity decreases notably in gema-, stanna-, and plumbapyramidanes (**III–V**). Within the latter group, the decrease in V_{cl} from **III** to **V** is more gradual. To understand this trend, it is important to consider that electrostatic interactions increase with the size of charges but decrease when the distance increases. Here, it is thus the elongation of the E–[$C_4(SiMe_3)_4$] distance which attenuates classical interactions according to Coulomb's law, even as the charges remain relatively stable.

Conversely, the V_{xc} contribution, which directly reflects the covalent interaction, exhibits a notably more stabilizing effect for **I** (-478.3 kcal mol^{-1}) as compared to **II–V** (ranging between -233.7 and -271.4 kcal mol^{-1}). This observation aligns with the previously discussed more covalent nature of the apex-base interaction in **I**. Furthermore, V_{xc} reveals pronounced distinctions within the more polar **II–V** series. Specifically, it decreases as one moves down the group, indicating weaker covalent interactions, with one notable exception: silapyramidane **II**. In this instance, V_{xc} is significantly less attractive than for **I** and **III**, diverging from the expected trend. Such anomalous behavior also correlates with some distinctive characteristics typically observed in C–Si compounds, which has also been related to the controversial charge-shift bonds.[52] Further independent support for this specificity can be found in that the electronegativity of Si is lower than that of Ge.

As expected, the covalent contributions correlate with the values of the delocalization indices (DIs), which are associated to the number of electron pairs shared between two basins. Namely, the DI between E and the $C_4(SiMe_3)_4$ group is 3.19 for **I**, ranging between 2.13 and 2.50 for **II** to **V**, in agreement with their much larger polar character. When comparing the bonding pattern of the latter group, significant differences are unveiled, in the same line as those revealed by V_{xc}. The DIs can be grouped into two sets: **II**, with a value of 2.13, and **III–V**, in which it ranges between 2.46 and 2.50. Again, and consistently, this reveals a higher degree of covalency in the latter group, driven by higher electron pair sharing. In this regard, it is again worth noting that the V_{xc} energy contribution is, in a first approximation, inversely proportional to the bond distance, this justifying why, while the DI of **III–V** is nearly the same, as the E–[$C_4(SiMe_3)_4$] distance increases its exchange-correlation attraction weakens.

The total interaction energy of both fragments, E_{int}, emerges as most stabilizing for **II** (-635.0 kcal mol^{-1}), wherein the significantly higher classical contribution compensates for a relatively lower covalent interaction. Following this, **I** (-439.8 kcal mol^{-1}) presents an inverse scenario, where V_{xc} counterbalances the positive value of V_{cl}. Subsequently, E_{int} exhibits a gradual decrease from **III** (-384.2 kcal mol^{-1}) to **V** (-298.9 kcal mol^{-1}), attributed to the weakening of both V_{cl} and V_{xc}.

The analysis of the interaction between the apex atom and the C atoms in the base (E–C) is consistent with previous results on the E–[$C_4(SiMe_3)_4$] interaction; that is, the E–C interaction in **I** is highly covalent (at least when compared to all the other cases under study), with a DI of 0.75 and a V_{xc} interaction of -114.3 kcal mol^{-1}.

Notice that this DI supports the naïve electron count coming from Wade-Mingos-Rudolph's rules, as it corresponds to the 3 electron pairs for the E–$C_4(SiMe_3)_4$] bonding divided by the 4 hypothetical chemical bonds taking place.

The DI sharply decreases for **II** (0.48), and then increases for **III–V** (0.55–0.57), which according to the Wade-Mingos-Rudolph's rules, would point to a decrease in the number of bonding electrons between the base and the apex atom and of the multicenter nature of this interaction. With respect to V_{xc}, we note that, as it is highly affected by the E–C distance (in addition to the number of electron pairs shared between both atoms), the results are probably less intuitive in terms of qualitative bond characterization. Be that as it may, they reveal weak although relevant covalent interactions in **II–V** (between -54.3 and -63.8 kcal mol^{-1}). These results correlate with reports from Andrada and co–workers, who, based on EDA calculations found important orbital contributions in the Si–C interaction in **II**, independently of whether silicon is considered as Si(0) or Si(II).[12]

At this point, we should also note that the above explained results put forward a high degree of polarity for the bonding in **II–V**, which is in agreement with previous analyses performed by resorting to QTAIM framework. Namely, bonding paths have been found for the E–C interactions.[11–14] Such results are also reproduced by us, as shown in Figure S7 and Table S12 for the $\mathbf{I_a}$–$\mathbf{V_a}$ model systems. The E–C interaction in $\mathbf{II_a}$–$\mathbf{V_a}$ is characterized by small electron density values, $\rho(r)$, (0.05–0.08 a.u.), and positive Laplacian of the electron density, $\nabla^2\rho(r)$, (0.13–0.14 a.u.) at the bond critical point, indicative of extreme bond

polarization. This behavior differs from that observed in $\mathbf{I}_a$, which shows a large electron density (0.172 a.u.) and negative Laplacian (−0.047 a.u.).[11]

Additional insight, particularly on multicenter-bonding and the presence of lone pairs (LPs), can be obtained through the Laplacian and the ELF functions. Figure 3 shows isocontours of $\nabla^2\rho(r)$ and isosurfaces of ELF for systems $\mathbf{I}_a$, $\mathbf{II}_a$, and $\mathbf{V}_a$ as representative examples. More details can be found in the supplementary information, Figures S3, S5 and S6, and Tables S10 and S11. The Laplacian of $\rho(r)$ had been reported to show the presence of a LP at the apex atom of **II**.[12] As shown here, this is also the case in $\mathbf{I}_a$ and $\mathbf{II}_a$, while the transition in the rest of the systems to a closed-shell regime is accompanied by considerably more spherical electron distributions around E, although a Natural Resonance Theory (NRT) analysis in Ref. [14] locates LPs also in these cases.

The ELF unveils that the apex atoms of $\mathbf{I}_a$ and $\mathbf{II}_a$ are engaged in 3c,2e trisynaptic interactions with each of the pair of C atoms forming one of the triangular faces of the pyramid. Also, four weakly populated 2c bond basins appear between E and each of the C atoms of the base. $\mathbf{I}_a$ and $\mathbf{II}_a$ also display lone-pair-like valence basins pointing outwards the axis of the pyramid, very populated in $\mathbf{I}_a$. The trisynaptic domains disappear in $\mathbf{III}_a$–$\mathbf{V}_a$, but monosynaptic C basins in the base remain with a very small population. A clear evolution towards sphericity (less hybrid character) of the apex LPs is also seen on moving down the group. At the ELF isovalue chosen (0.75), the LP in $\mathbf{V}_a$ cannot be discerned, supporting its absence in the Laplacian plot.

The effect of the E atom on the electronic structure of the base was also analyzed by comparing the C–C interactions within the complex and those in the free doubly charged cyclobutadiene-derivative $[C_4(SiMe_3)_4]^{2-}$. Note that, because of electron delocalization within the ring, there are significant electron pair interactions not only between adjacent C atoms in the ring (C–C interactions in Table 2) but also between C atoms that occupy opposite positions (denoted as C–C′ in Table 2). DIs for adjacent C–C interactions are higher than 1, showing a clear partial double bond character, while non-adjacent DIs take non-negligible values between 0.18 and 0.22. It is noteworthy that the base of **II** displays DI values very close to those of $[C_4(SiMe_3)_4]^{2-}$. Namely, the DI for adjacent C–C interactions in **II** and $[C_4(SiMe_3)_4]^{2-}$ take values of 1.24 and 1.28, respectively, while the values for apposite interactions are 0.22 and 0.26. We recall here that C–C′ DIs, which in a six-member ring would be equivalent to the so-called *para*-delocalization indices (PDI) have been successfully used as descriptors of aromaticity.[53] In the same line, V_{xc} takes very similar values for both systems (−226.6 and −224.4 kcal mol^{-1}, respectively). This is a very strong indication of similar electronic structures in $[C_4(SiMe_3)_4]^{2-}$ (which exhibits a very high degree of electron delocalization) and the base of complex **II**.

We now focus on complexes **III**, **IV** and **V**, for which there is a decrease in V_{xc} and DI with respect to **II**, with similar values in the three cases, about −218 kcal mol^{-1} and 1.20, respectively (see Table 2). In broad strokes, we attribute this effect to stronger E–$[C_4(SiMe_3)_4]^{2-}$ covalent interactions (characterized by higher DIs and V_{xc}, *vide supra*), which are translated into lower electron density remaining in the base. Higher covalency in **I** is also clearly revealed by an important decrease in the DI and V_{xc} values for adjacent C–C bonds, having a DI of 1.11 and a V_{xc} interaction term of −206.5 kcal mol^{-1}; which derives from more effective electron sharing in E–C bonds.

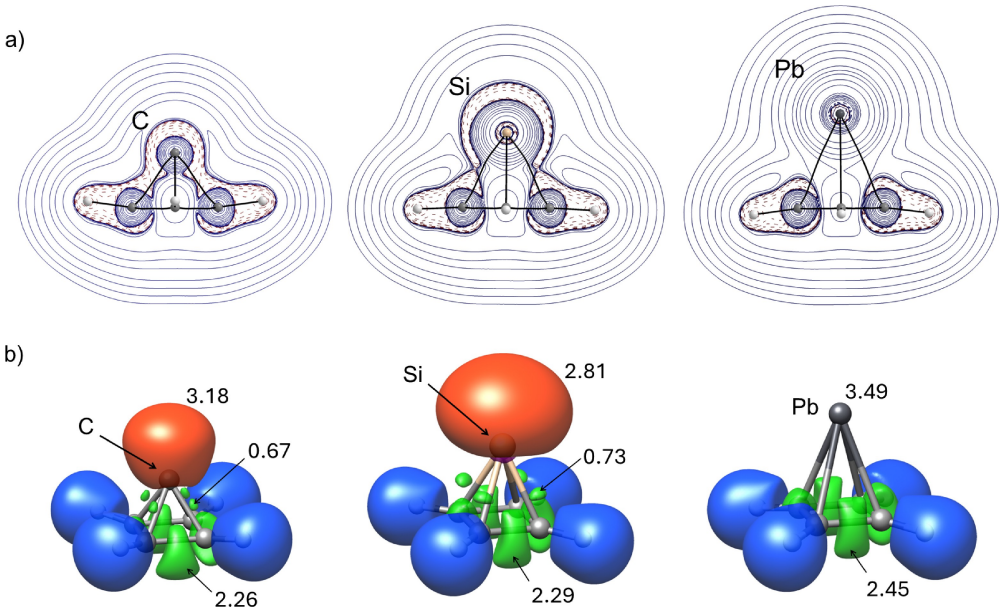

Figure 3. a) Laplacian function isocontours on a plane containing a diagonal of the base and the apex atom (solid-blue positive, dashed-red, negative); and b) ELF isosurfaces (with isovalue 0.75) for the $\mathbf{I}_a$, $\mathbf{II}_a$ and $\mathbf{V}_a$ systems. In green: disynaptic and trisynaptic basins; blue: C–H bond basins; purple: core basins; and orange: monosynaptic basins). ELF populations (in number of electrons) of the monosynaptic V(E), trisynaptic V(C,C,E) and disynaptic V(C,E) basins are also provided. Note that for the selected isovalue most of the basins do not appear for $\mathbf{V}_a$ (see Figure S6 for other isovalues).

As the aromaticity of the base is regarded, besides the C–C′ DI, we have computed several other aromaticity indices: HOMA, FLU and MCI.[54,55] They are found in Tables S14 and S15. Due to their reference-free nature, we prefer to rely on both the MCI and DI. As it can be seen from the Tables, these descriptors fluctuate slightly with the conformer and the substituent R, depending mainly on the nature of the apex atom E. It is satisfying that, according to MCI, the C and Si bases are the least and most aromatic of all, respectively, and that the group **III–V** is pretty homogeneous in this regard, with significant aromatic MCIs around 0.023 and C–C′ DIs of 0.18–0.19. It is remarkable to note that the significant aromatic character of the pyramidane base revealed by these measures are also in line with NICS, NICS(1) and NICS(1)$_{zz}$ calculations performed by other authors, which point towards significant π-delocalization (and thus aromatic character) in the C_4-base.[11,14]

All in all, the combined EDF/IQA approach shows how both the electron counting perspective provided by the EDF method, which leads to numerous population-related descriptors, and the detailed local energetic view provided by IQA can be put to work together to unveil, from the orbital invariant analysis of a given wavefunction, both the nature of the chemical bonding in an exotic scenario and the plausibility of aromaticity of a given fragment of a molecule. This has been shown to be the case in Si[$C_4(SiMe_3)_4$], which is well described, broadly speaking, as an aromatic dianion coupled mostly electrostatically to a Si dication.

Conclusions

Much theoretical work has been done in the past to elucidate the exotic bonding regime displayed by compounds belonging to the the [4]-pyramidane family. In the case of the E$C_4(SiMe_3)_4$ set, E=C, Si, Ge, Sn, Pb, labelled as **I–V**, most works agree on a transition from a covalent interaction between the E apex atom and the remaining fragment (the base) to a very polar one with considerable electrostatic component as we transition down the group. Many also point out the relevant role that the aromaticity of the base might play. Unfortunately, the methods that are typically used to deal with covalency/ionicity and aromaticity are not usually compatible, leading to unreliable conclusions. We have shown how quantum chemical topology tools, like those provided by the electron distribution functions (EDFs), multicenter indices (MCI), and the interacting quantum atoms approach (IQA), which analyze the electronic structure of a system and its energetic interactions using a common orbital invariant framework can be used to provide a consistent set of results for all these properties. In this case, our results agree well with previous proposals. In **I** and in **III–V**, the apex-base interaction evolves smoothly from covalent to very polar, while in **II** we find a system in which the Si atom donates two electrons to the base, whose local electronic structure becomes very close to that of an isolated $[C_4(SiMe_3)_4]^{2-}$ aromatic anion.

Computational Details

DFT calculations were performed by using the Gaussian 16[56] and Orca 5.0[57] software packages. Geometry optimizations of pyramidanes **I**, **II** and **III**, as well as $[C_4(SiMe_3)_4]^{2-}$ anion were conducted with the B3LYP exchange-correlation functional,[58] in conjunction with D3BJ empirical dispersion correction scheme,[59] and the Ahlrichs def2-TZVP basis sets,[60] as implemented in Gaussian 16. In order to perform all-electron calculations for stanna- and plumbapyramidanes (**IV** and **V**, respectively), we optimized their geometries at the B3LYP–D3BJ level, in conjunction with the zeroth order regular approximation (ZORA) to take into account relativistic effects.[61] In the former case, we considered the SARC-ZORA-TZVP basis set for Sn and Pb, and the SARC/J auxiliary basis sets[62] together with the RIJCOSX approximation to accelerate the calculations.[63] Geometries of **IV** and **V** were also optimized by using the def2-TZVP basis set with electron core potentials (ECP), and showed marginal differences with respect to those obtained with the ZORA approximation (Pb–C and Sn–C distances differ about 0.01 Å). Given this minor differences, we used this methodology to compute geometries of **I–V** with the M06,[64] M06-L[65] and TPSSh[66] functionals. Note that, given the smooth potential energy surface of the systems, we needed to freeze methyl groups in the trimethylsilyl groups in some cases, as explained in the Supporting Information. E[C_4H_4] and E[$C_4(SiH_3)_4$] families of systems were also computed at the B3LYP–D3BJ/def2-TZVP level of theory (including ZORA framework for Sn and Pb atoms).

EDF calculations were performed by means of the EDF program[50b] and IQA, QTAIM, and MEP analysis was carried out with the AIMALL software.[67] ELF calculations were carried out with TopMod.[68] In all cases we used the corresponding B3LYP pseudo-single-determinant Kohn-Sham wavefunctions. Aromaticity indices were computed with ESI-3D.[53] Graphical representations were performed with VESTA.[69]

Supporting Information Summary

The supporting information contains: raw energy data, structural parameters for compounds **I–V** in geometry #2, Laplacian isocontours, ELF and MEP isosurfaces, molecular graphs and densities and Laplacians at bond critical points for systems $\mathbf{I_a}$–$\mathbf{V_a}$. Also EDF and IQA results for systems **I–V** in geometry #2, and aromaticity indices for $\mathbf{I_a}$–$\mathbf{V_a}$ and $\mathbf{I_b}$-$\mathbf{V_b}$, together with Cartesian coordinates for all of the systems.

Acknowledgements

The authors acknowledge the Spanish *"Ministerio de Ciencia, Innovación y Universidades"* for financial support (PID2021–122763NB–I00 and PID2022–140244NB–I00 and RYC-2017–22853), as well as the *"Fundación para el Fomento en Asturias de la Investigación Científica Aplicada y la Tecnología* (FICyT)" (IDI-2021–000054) and the *"Departamento de Educación, Ciencia y*

Universidades del Gobierno de Aragón" (group E42_20R). D. B.-E. acknowledges FICyT for a predoctoral grant (PA-23-BP22–168). Technical support from the *Instituto de Biocomputación y Física de Sistemas Complejos* (Universidad de Zaragoza) are also acknowledged.

Conflict of Interests

The authors declare no conflict of interest.

Data Availability Statement

The data that support the findings of this study are available in the supplementary material of this article.

Keywords: Pyramidanes · Quantum chemical topology · Chemical bonding · Group 14 compounds · Energy decomposition

[1] H. W. Kroto, J. R. Heath, S. C. O'Brien, R. F. Curl, R. E. Smalley, *Nature* **1985**, *318*, 162–163.
[2] Q. Sun, C. Mück-Lichtenfeld, G. Kehr, G. Erker, *Nat. Rev. Chem.* **2023**, *7*, 732–746.
[3] V. I. Minkin, R. M. Minyaev, I. I. Zakharov, V. I. Avdeev, *Zh. Org. Khim.* **1978**, *14*, 3.
[4] K. Wiberg, *Chem. Rev.* **1989**, *89*, 975–983.
[5] V. I. Minkin, R. M. Minyaev, G. V. Orlova, *J. Mol. Struct.* **1984**, *110*, 241–253.
[6] V. Balaji, J. Michl, *Pure Appl. Chem.* **1988**, *60*, 189.
[7] E. Lewars, *J. Mol. Struct.* **1998**, *423*, 173–188.
[8] E. Lewars, *J. Mol. Struct.* **2000**, *507*, 165–184.
[9] J. P. Kenny, K. M. Krueger, J. C. Rienstra-Kiracofe, H. F. Schaefer III, *J. Phys. Chem. A.* **2001**, *105*, 7745–7750.
[10] M. G. Rosenberg, U. H. Brinker, *J. Org. Chem.* **2021**, *86*, 878–891.
[11] V. Y. Lee, O. A. Gapurenko, *Chem. Commun.* **2023**, *59*, 10067–10086.
[12] T. Imagawa, L. Giarrana, D. M. Andrada, B. Morgenstern, M. Nakamoto, D. Scheschkewitz, *J. Am. Chem. Soc.* **2023**, *145*, 4757–4764.
[13] V. Y. Lee, Y. Ito, A. Sekiguchi, H. Gornitzka, O. A. Gapurenko, V. I. Minkin, R. M. Minyaev, *J. Am. Chem. Soc.* **2013**, *135*, 8794–8797.
[14] V. Y. Lee, O. A. Gapurenko, Y. Ito, T. Meguro, H. Sugasawa, A. Sekiguchi, R. M. Minyaev, V. I. Minkin, R. H. Herber, H. Gornitzka, *Organometallics* **2016**, *35*, 346–356.
[15] a) G. Anderson, J. C. Green, M. D. Francis, *Organometallics* **2003**, *22*, 2897–2901; b) M. D. Francis, P. B. Hitchcock, *Organometallics* **2003**, *22*, 2891–2896; c) M. D. Francis, P. B. Hitchcock, *Chem. Commun.* **2001**, *1*, 86–87; d) J. M. Lynam, M. C. Copsey, M. Green, J. C. Jeffery, J. E. McGrady, C. A. Russell, J. M. Slattery, A. C. Swain, *Angew. Chem. Int. Ed.* **2003**, *42*, 2778–2782.
[16] P. Coburger, F. Masero, J. Bösken, V. Mougel, H. A. Grützmacher, *Angew. Chem., Int. Ed.* **2022**, *61*, e202211749.
[17] S. Masamune, M. Sakai, H. Ona, *J. Am. Chem. Soc.* **1972**, *94*, 8955–8956.
[18] S. Masamune, M. Sakai, H. Ona, A. J. Jones, *J. Am. Chem. Soc.* **1972**, *94*, 8956–8958.
[19] V. Y. Lee, H. Sugasawa, O. A. Gapurenko, R. M. Minyaev, V. I. Minkin, H. Gornitzka, A. Sekiguchi, *Chem. Eur. J.* **2016**, *22*, 17585–17589.
[20] Q. Sun, C. G. Daniliuc, X. Yu, C. Mück-Lichtenfeld, G. Kehr, G. Erker, *J. Am. Chem. Soc.* **2022**, *144*, 7815–7821.
[21] V. Y. Lee, H. Sugasawa, O. A. Gapurenko, R. M. Minyaev, V. I. Minkin, H. Gornitzka, A. Sekiguchi, *J. Am. Chem. Soc.* **2018**, *140*, 6053–6056.
[22] P. Coburger, *Eur. J. Inorg. Chem.* **2024**, *27*, e202300596.
[23] R. F. W. Bader, *Atoms in Molecules: A Quantum Theory*, Clarendon Press, Oxford **1990**.
[24] K. Torstensen, A. Ghosh, *ACS. Org. Inorg. Au.* **2024**, *4*, 102–105.
[25] D. L. Luder, N. Terefenko, Q. Sun, H. Eckert, C. Mück-Lichtenfeld, G. Kehr, G. Erker, T. Wiegand, *Chem. Eur. J.* **2024**, *30*, e202303701.
[26] A. D. Becke, K. E. Edgecombe, *J. Chem. Phys.* **1990**, *92*, 5397–5403.
[27] H. Fallah-Bagher-Shaidaei, C. S. Wannere, C. Corminboeuf, R. Puchta, P. V. R. Schleyer, *Org. Lett.* **2006**, *8*, 863–866.
[28] L. Zhao, M. von Hopffgarten, D. M. Andrada, G. Frenking, *Wiley Interdiscip. Rev.: Comput. Mol. Sci.* **2018**, *8*, 1–37.
[29] a) K. Wade, *J. Chem. Soc. D.* **1971**, *15*, 792–793; b) R. W. Rudolph, *Acc. Chem. Res.* **1976**, *9*, 446–452; c) D. M. P. Mingos, *Acc. Chem. Res.* **1984**, *17*, 311–319.
[30] a) K. Takanashi, A. Inatomi, V. Y. Lee, M. Nakamoto, M. Ichinohe, A. Sekiguchi, *Eur. J. Inorg. Chem.* **2008**, *2008*, 1752–1755; b) A. Sekiguchi, T. Matsuo, H. Watanabe, *J. Am. Chem. Soc.* **2000**, *122*, 5652–5653.
[31] a) A. Efraty, *Chem. Rev.* **1977**, *77*, 691–744; b) K. Takanashi, V. Y. Lee, Akira Sekiguchi, *Organometallics* **2009**, *28*, 1248–1251; c) D. Seyferth, *Organometallics* **2003**, *1*, 2–20.
[32] a) J. T. Boronski, S. T. Liddle, *Eur. J. Inorg. Chem.* **2020**, *2020*, 2851–2861; b) J. T. Boronski, L. R. Doyle, J. A. Seed, A. J. Wooles, *Angew. Chem. Int. Ed.* **2020**, *59*, 295–299; c) J. T. Boronski, A. J. Wooles, S. T. Liddle, *Chem. Sci.* **2020**, *11*, 6789–6794.
[33] P. L. A. Popelier, *Intermolecular Forces and Clusters I*, Springer, Berlin, Heidelberg **2005**, 1.
[34] M. A. Blanco, A. Martín Pendás, E. Francisco, *J. Chem. Theory Comput.* **2005**, *1*, 1096–1109.
[35] A. Martin Pendás, J. L. Casals-Sainz, E. Francisco, *Chem. Eur. J.* **2019**, *25*, 309–314.
[36] a) A. Martín Pendás, E. Francisco, D. Suárez, A. Costales, N. Díaz, J. Munárriz, T. Rocha-Rinza, J. M. Guevara-Vela, *Phys. Chem. Chem. Phys.* **2023**, *25*, 10231–10262; b) J. M. Guevara-Vela, E. Francisco, T. Rocha-Rinza, Á. Martín Pendás, *Molecules* **2020**, *25*, 4028.
[37] a) A. Pérez-Bitrián, J. Munárriz, J. S. Sturm, D. Wegener, K. B. Krause, A. Wiesner, C. Limberg, S. Riedel, *Inorg. Chem.* **2023**, *62*, 12947–12953; b) A. Pérez-Bitrián, J. Munarriz, K. B. Krause, J. Schlögl, K. F. Hoffmann, J. S. Sturm, A. N. Hadi, C. Teutloff, A. Wiesner, C. Limberg, S. Riedel, *Chem. Sci.* **2024**, *15*, 5564–5572.
[38] a) J. M. Guevara-Vela, K. Hess, T. Rocha-Rinza, A. Martín Pendás, M. Flores-Álamo, G. Moreno-Alcántar, *Chem. Commun.* **2022**, *58*, 1398–1401; b) A. Caballero-Muñoz, J. M. Guevara-Vela, A. Fernández-Alarcón, M. A. Valentín-Rodríguez, M. Flores-Álamo, T. Rocha-Rinza, H. Torrens, G. Moreno-Alcántar, *Eur. J. Inorg. Chem.* **2021**, *2021*, 2702–2711.
[39] S. Sowlati-Hashjin, V. Šadek, S. A. Sadjadi, M. Karttunen, A. Martín-Pendás, C. Foroutan-Nejad, *Nat. Commun.* **2022**, *13*, 2069.
[40] X. Fradera, M. A. Austen, R. F. W. Bader, *J. Phys. Chem. A.* **1999**, *103*, 304–314.
[41] A. Martín Pendás, E. Francisco, *Phys. Chem. Chem. Phys.* **2018**, *20*, 16231–16237.
[42] M. Giambiagi, M. Segre de Giambiagi, C. D. dos Santos Silva, A. Paiva de Figueiredo, *Phys. Chem. Chem. Phys.* **2000**, *2*, 3381–3392.
[43] a) A. Martín Pendás, E. Francisco, M. A. Blanco, *J. Chem. Phys.* **2007**, *127*, 144103; b) A. Martín Pendás, E. Francisco, M. A. Blanco, *Phys. Chem. Chem. Phys.* **2007**, *9*, 1087–1092.
[44] Á. Martín Pendás, E. Francisco, *ChemPhysChem.* **2019**, *20*, 2722–2741.
[45] a) J. Munarriz, E. Velez, M. A. Casado, V. Polo, *Phys. Chem. Chem. Phys.* **2018**, *20*, 1105–1113; b) D. Barrena-Espés, J. Munárriz, Á. Martín Pendás, *J. Chem. Phys.* **2024**, *160*, 144106.
[46] a) G. W. Breton, K. L. Martin, *J. Org. Chem.* **2002**, *67*, 6699–6704; b) B. A. Hess, C. S. Ewig, L. J. Schaad, *J. Org. Chem.* **1985**, *50*, 5869–5871; c) Y. Jung, T. Heine, P. V. R. Schleyer, M. Head-Gordon, *J. Am. Chem. Soc.* **2004**, *126*, 3132–3138; d) G. van Zandwijk, R. A. J. Janssen, H. M. Buck, *J. Am. Chem. Soc.* **1990**, *112*, 4155–4164; e) M. Balci, M. L. McKee, P. V. R. Schleyer, *J. Phys. Chem. A.* **2000**, *104*, 1246–1255.
[47] P. Pyykkö, *J. Phys. Chem. A.* **2015**, *119*, 2326–2337.
[48] A. E. Reed, R. B. Weinstock, F. Weinhold, *J. Chem. Phys.* **1985**, *83*, 735–746.
[49] A. J. Stone, *J. Phys. Chem. A.* **2017**, *121*(7), 1531–1534.
[50] a) E. Francisco, A. Martín Pendás, M. A. Blanco, *J. Chem. Phys.* **2007**, *126*, 094102; b) E. Francisco, A. Martín Pendás, M. A. Blanco, *Comput. Phys. Commun.* **2008**, *178*, 621–634.
[51] G. Frenking, R. Tonner, S. Klein, N. Takagi, T. Shimizu, A. Krapp, K. K. Pandeyc, P. Parameswaran, *Chem. Soc. Rev.* **2014**, *43*, 5106–5139.
[52] S. Shaik, D. Danovich, J. Morrison Galbraith, B. Braïda, W. Wu, P. C. Hiberty, *Angew. Chem. Int. Ed.* **2020**, *59*, 984–1001.
[53] J. Poater, X. Fradera, M. Duran, M. solà, *Chem. Eur. J.* **2003**, *9*, 400–406.
[54] Matito E., ESI-3D: Electron Sharing Indexes Program for 3D Molecular Space Partitioning. http://iqc.udg.es/~eduard/ESI. Girona, IQC **2006**.
[55] a) F. Feixas, E. Matito, J. Poater, M. Solà, *Chem. Soc. Rev.* **2015**, *44*, 6434–6451; b) E. Matito, *Phys. Chem. Chem. Phys.* **2016**, *18*, 11839–11846; c) F.

Feixas, E. Matito, J. Poater, M. Solà, *J. Phys. Chem. A.* **2007**, *111*, 4513–4521; d) I. Casademont-Reig, E. Ramos-Cordoba, M. Torrent-Sucarrat, E. Matito, Aromaticity descriptors based on electron delocalization. In Book: *Aromaticity, Modern Computational Methods and Applications* (Ed: Israel Fernández), Elsevier, The Netherlands **2021**.

[56] M. J. Frisch, G. W. Trucks, H. B. Schlegel, G. E. Scuseria, M. A. Robb, J. R. Cheeseman, G. Scalmani, V. Barone, G. A. Petersson, H. Nakatsuji, X. Li, M. Caricato, A. V. Marenich, J. Bloino, B. G. Janesko, R. Gomperts, B. Mennucci, H. P. Hratchian, J. V. Ortiz, A. F. Izmaylov, J. L. Sonnenberg, D. Williams-Young, F. Ding, F. Lipparini, F. Egidi, J. Goings, B. Peng, A. Petrone, T. Henderson, D. Ranasinghe, V. G. Zakrzewski, J. Gao, N. Rega, G. Zheng, W. Liang, M. Hada, M. Ehara, K. Toyota, R. Fukuda, J. Hasegawa, M. Ishida, T. Nakajima, Y. Honda, O. Kitao, H. Nakai, T. Vreven, K. Throssell, J. A. Montgomery Jr., J. E. Peralta, F. Ogliaro, M. J. Bearpark, J. J. Heyd, E. N. Brothers, K. N. Kudin, V. N. Staroverov, T. A. Keith, R. Kobayashi, J. Normand, K. Raghavachari, A. P. Rendell, J. C. Burant, S. S. Iyengar, J. Tomasi, M. Cossi, J. M. Millam, M. Klene, C. Adamo, R. Cammi, J. W. Ochterski, R. L. Martin, K. Morokuma, O. Farkas, J. B. Foresman, D. J. Fox, Gaussian 16, revision C.01; Gaussian, Inc., Wallingford, CT **2016**.

[57] a) F. Neese, *WIREs Comput. Mol. Sci.* **2022**, *12*, e1606; b) F. Neese, *WIREs Comput. Mol. Sci.* **2012**, *2*, 73–78.

[58] A. D. Becke, *J. Chem. Phys.* **1993**, *98*, 1372–1377.

[59] a) S. Grimme, J. Antony, S. Ehrlich, H. Krieg, *J. Chem. Phys.* **2010**, *132*, 154104; b) E. R. Johnson, A. D. Becke, *J. Chem. Phys.* **2005**, *123*, 024101.

[60] F. Weigend, R. Ahlrichs, *Phys. Chem. Chem. Phys.* **2005**, *7*, 3297–3305.

[61] a) E. van Lenthe, E. J. Baerends, J. G. Snijders, *J. Chem. Phys.* **1993**, *99*, 4597–4610; b) E. van Lenthe, J. G. Snijders, E. J. Baerends, *J. Chem. Phys.* **1996**, *105*, 6505–6516.

[62] a) J. D. Rolfes, F. Neese, D. A. Pantazis, *J. Comput. Chem.* **2020**, *41*, 1842–1849; b) D. A. Pantazis, F. Neese, *Theor. Chem. Acc.* **2012**, *131*, 1292; c) D. A. Pantazis, X. Y. Chen, C. R. Landis, F. Neese, *J. Chem. Theory Comput.* **2008**, *4*, 908–919.

[63] B. Helmich-Paris, B. De Souza, F. Neese, R. Izsák, *J. Chem. Phys.* **2021**, *155*, 104109.

[64] Y. Zhao, D. G. Truhlar, *Theor. Chem. Acc.* **2008**, *120*, 215–241.

[65] Y. Zhao, D. G. Truhlar, *J. Chem. Phys.* **2006**, *125*, 194101.

[66] a) J. Tao, J. P. Perdew, V. N. Staroverov, G. E. Scuseria, *Phys. Rev. Lett.* **2003**, *91*, 146401; b) V. N. Staroverov, G. E. Scuseria, J. Tao, J. P. Perdew, *J. Chem. Phys.* **2003**, *119*, 12129–12137.

[67] AIMAll (Version 19.10.12), Todd A. Keith, TK Gristmill Software, Overland Park KS, USA **2019**, aim.tkgristmill.com.

[68] S. Noury, X. Krokidis, F. Fuster, B. Silvi, *Comput. Chem.* **1999**, *23*, 597–604.

[69] K. Momma, F. Izumi, *J. Appl. Crystallogr.* **2011**, *44*, 1272–1276.

Manuscript received: March 22, 2024
Revised manuscript received: July 18, 2024
Accepted manuscript online: July 23, 2024
Version of record online: ■■, ■■

RESEARCH ARTICLE

The [4]-pyramidane $E[C_4(SiMe_3)_4]$ (E═C, Si, Ge, Sn, Pb) family is studied, focusing on the characterization of the interaction between the pyramid apex (E) and the cyclobutadiene-based base. Orbital invariant techniques based on Quantum Chemical Topology, including QTAIM and ELF analyses, electron distribution functions (EDFs), and IQA energetic decompositions are used.

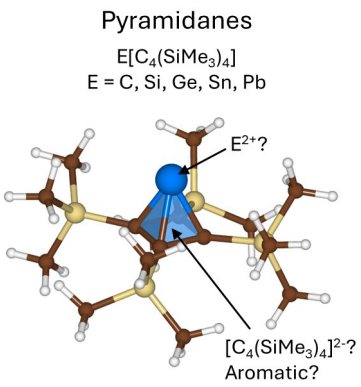

L. Vidal, D. Barrena-Espés, J. Echeverría, J. Munárriz, Á. M. Pendás**

1 – 11

Deciphering Pyramidanes: A Quantum Chemical Topology Approach